Tele-Running: Trajectory Generation for Monopod Robots by Teleoperation

David Wandinger[1], Annika Schmidt[1,2], Antonin Raffin[1], Alin Albu-Schäffer[1,2], and Manuel Keppler[1]

***Abstract*— Energy-efficient legged locomotion in robots depends on exploiting passive dynamics, particularly with integrated mechanical compliance. Traditional model-based control strategies that leverage these dynamics often encounter challenges due to inherent model uncertainties. We propose a novel model-free method for generating motor trajectories in compliantly actuated monopods using teleoperation with force feedback. This approach allows operators to detect ground reaction forces and excite the robot's natural frequency, achieving highly efficient hopping. The method results in a mechanical Cost of Transport (CoT) of 0.25 at $0.63\,\mathrm{m\,s^{-1}}$ on an articulated hopper. To further enhance energy efficiency and adjust for hardware variations, these trajectories are refined using Black-Box Optimization (BBO) directly on the hardware. Experimental results confirm that these optimized trajectories closely match the efficiency of those initiated by humans, demonstrating the effectiveness of this method in exciting the robot's natural dynamics.**

I. Introduction

The research in legged robot locomotion is of increasing importance as mobile robots have proven to be valuable assets in many areas including exploration or search and rescue. These tasks are commonly in an uncertain and rough terrain where wheeled robots can not navigate. Monopods, i.e. one-legged robots, offer a way to reduce the complexity in studying legged locomotion while still getting valuable insight into controlling these robots.

Great advancements in the design and control of monopods have been made with the introduction of dynamic balance by Raibert [1]. Monopods controlled by dynamic balance are equipped with elastic actuators and use passive dynamics, such as the Atrias robot [2]. Intrinsic elasticity is a key element in the design because it has useful dynamic properties for legged locomotion. Elastic monopods are robust against impacts and can store and release energy which results in an inherent oscillatory behavior.

These characteristics can be used to make legged locomotion energy efficient. A common metric for this is the Cost of Transport (CoT) which relates traversed distance and consumed energy of the robot. State-of-the-art elastic monopods are the ARL Monopod I and II [3], [4] and SPEAR [5]. Their respective CoT is shown in Fig. 1 in comparison to the Quadruped MIT Cheetah [6].

This project has received funding from the European Research Council (ERC) under the European Union's Horizon 2020 research and innovation programme (grant agreement No. 835284).

[1]Institute of Robotics and Mechatronics, German Aerospace Center (DLR), 82234 Oberpfaffenhofen, Germany, david.wandinger@dlr.de .

[2]Department of Informatics, Technical University of Munich (TUM), 85748 Garching, Germany.

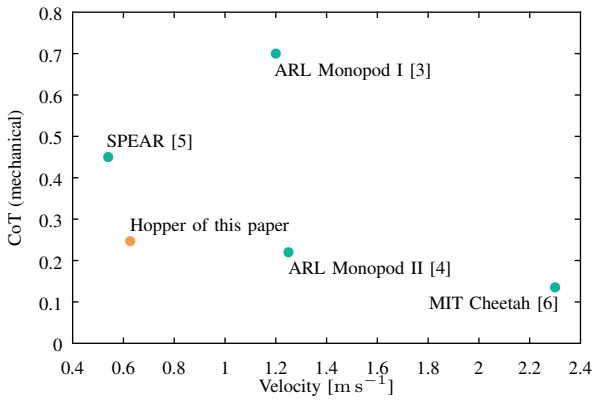

Fig. 1. Kármán-Gabrielli diagram for state-of the-art elastic legged robots.

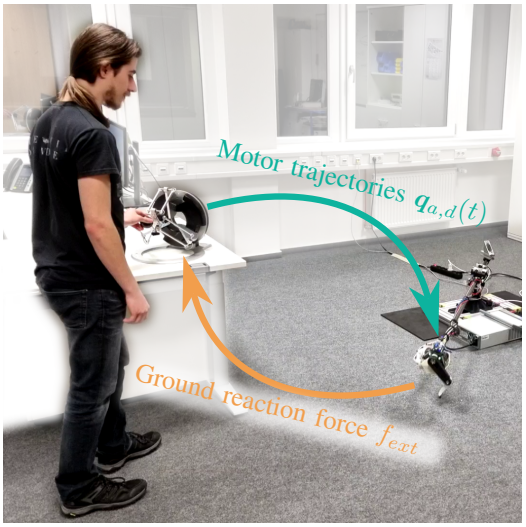

Fig. 2. Operator controlling the hopper by commanding motor trajectories using teleoperation with force feedback to sense the ground reaction force.

In order to generate energy-efficient locomotion with these systems, the controller should exploit the intrinsic elasticity [7], [8]. To achieve this, many controllers are based on the model of a Spring-Loaded Inverted Pendulum (SLIP) [9], [10], [11]. This model is especially useful for analyzing hopping and running [12]. The SLIP model can be used to identify cyclic motions that use the passive dynamics of the robot by analyzing nonlinear modes [13]. Strategies such as offline optimization and inverse dynamics are popular approaches to generate trajectories that use the passive dynamics of the robot [14], [15]. Many monopods are designed

to be close to an ideal SLIP. For robots with articulated joints the SLIP model can be applied by feedback model matching [16], [17].

However, shaping the dynamics of a robot comes with increased control effort, the need for an accurate model and may not be feasible if the mechanical design deviates much from an ideal SLIP model [18], [19]. The discussed control approaches are model-based and results rely heavily on hardware parameters such as friction and external forces. This complicates the transfer on hardware and there is no guarantee, that the resulting motion is energy efficient and is leveraging the passive dynamics of the robot.

The main idea of this work is to generate motor trajectories that exploit the passive dynamics of the monopod without the need for a model or dynamic shaping. The approach relies on the human's capability to excite nonlinear dynamics intuitively. We know this from experience, such as exciting the eigenfrequencies of a long beam when held in the hand, and experiments [20], [21]. We demonstrate an operator can generate energy-efficient hopping gaits on a compliantly actuated leg. To do so, adequate feedback is needed. We present a teleoperation setup that lets an operator directly control the robot's foot tip via the motor positions while force feedback is provided, which represents the robot's actual dynamics cf. Fig. 2.

The generated motor trajectories are evaluated based on the CoT of the resulting gait. The performance of the human generated trajectory is compared to a CoT optimal trajectory obtained by Black-Box Optimization (BBO) with the human generated motor trajectories as the initial value.

The paper is structured as follows. Section II will introduce the robot and its properties while the control via teleoperation and force feedback is described in Section III. Section IV will focus on the optimization for CoT and Section V will present the results. Conclusions are drawn in Section VI. A video of the hopper during teleoperation can be found here: `https://youtu.be/NUeaZ4gpSnU`

II. Mechanical Properties of the Controlled Robot

The considered robotic leg was developed as part of the DLR quadruped Bert. The leg features biarticular actuation, where the second joint is coupled through belts to make the overall dynamics closer to a SLIP, as discussed in its predecessor [22]. Its kinematics are depicted in Fig. 3 with basic parameters in Table I.

Throughout this paper, link coordinates are denoted by $\boldsymbol{q}_u \in \mathbb{R}^2$. The vector $\boldsymbol{x}_b \in \mathbb{R}^2$ describes the position of the floating base frame $\mathcal{B}$ w.r.t. the world frame $\mathcal{W}$. The robot is free to move in the $\mathcal{W}_{x,z}$-plane with its rotation about the $\mathcal{B}_y$-axis locked. The frame $\mathcal{F}$ is attached to the foot tip of the robot, with the same configuration independent orientation as $\mathcal{B}$. The position of the foot tip w.r.t. $\mathcal{B}$ is denoted by $\boldsymbol{x}_f$.

The dynamics of the robot are described by the equations of motions for floating base robots:

$$\boldsymbol{M}\begin{bmatrix}\ddot{\boldsymbol{x}}_b\\ \ddot{\boldsymbol{q}}_u\end{bmatrix}+\boldsymbol{C}\begin{bmatrix}\dot{\boldsymbol{x}}_b\\ \dot{\boldsymbol{q}}_u\end{bmatrix}+\boldsymbol{g}\;=\;\begin{bmatrix}\boldsymbol{0}\\ \boldsymbol{\tau}_j\end{bmatrix}+\begin{bmatrix}\boldsymbol{\mathcal{Q}}_{u,b}\\ \boldsymbol{\mathcal{Q}}_{u,j}\end{bmatrix}\;, \quad (1)$$

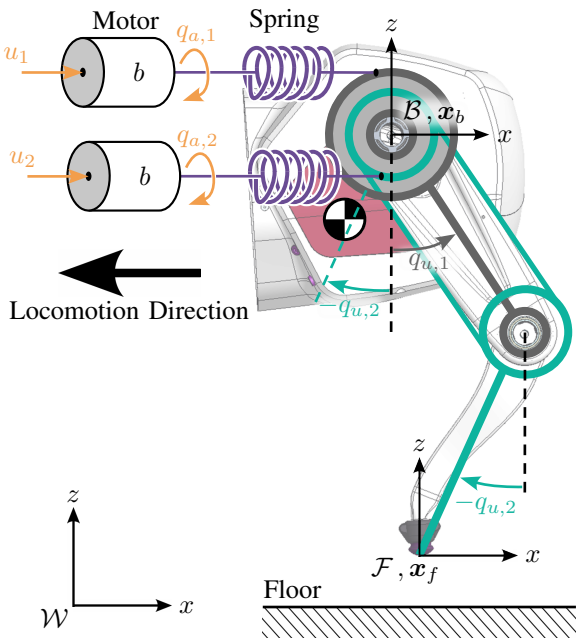

Fig. 3. Kinematics of the considered hopper with biarticular and serial elastic actuation.

TABLE I
Robot Parameters

Degrees of freedom:	Robot: 2	Base: 2
Robot mass m:	0.99	kg
Link length:	120	mm
Motor inertia b:	0.02	$\mathrm{kg\,m^2}$
Spring stiffness $\boldsymbol{K}$:	$\mathrm{diag}(2.95, 3.10)$	$\mathrm{N\,m\,rad^{-1}}$

where the inertia matrix $\boldsymbol{M}(\boldsymbol{q}_u) \in \mathbb{R}^{4\times4}$ determines inertial forces and torques on the robot's base and joints. The Coriolis/centrifugal matrix is denoted by $\boldsymbol{C}(\boldsymbol{q}_u, \dot{\boldsymbol{q}}_u) \in \mathbb{R}^{4\times4}$ and the gravity vector by $\boldsymbol{g}(\boldsymbol{q}_u) \in \mathbb{R}^4$. These are configuration-dependent. Throughout this paper, the arguments are omitted for brevity. External forces acting on the robot's joints and base are denoted by $\boldsymbol{\mathcal{Q}}_{u,j}$ and $\boldsymbol{\mathcal{Q}}_{u,b} \in \mathbb{R}^2$, respectively and $\boldsymbol{\tau}_j \in \mathbb{R}^2$ denotes the spring torques in both joints.

The joints are driven by Serial Elastic Actuators (SEAs) where the links and motors are decoupled by a mechanical spring. This makes the robot more robust against impacts and the kinetic energy stored in the springs can be used for energy-efficient locomotion. To this end, the joint torques follow the dynamics described by:

$$\boldsymbol{B}\ddot{\boldsymbol{q}}_a + \boldsymbol{\tau}_j = \boldsymbol{u} + \boldsymbol{\mathcal{Q}}_a\;, \quad (2)$$

with

$$\boldsymbol{\tau}_j = K\left(\boldsymbol{q}_a - \boldsymbol{q}_u\right)\;, \quad (3)$$

where the motor coordinates are denoted by $\boldsymbol{q}_a \in \mathbb{R}^2$ and the diagonal matrices $\boldsymbol{B}$ and $\boldsymbol{K} \in \mathbb{R}^{2\times2}$ contain the motor inertias and joint stiffnesses, respectively. The vector $\boldsymbol{\mathcal{Q}}_a \in \mathbb{R}^2$ denotes motor friction. Motor torques are represented by $\boldsymbol{u} \in \mathbb{R}^2$. They are commanded using a PID controller,

following the control law:

$$\boldsymbol{u} = -80\,(\boldsymbol{q}_a - \boldsymbol{q}_{a,d}) - 0.5\,\dot{\boldsymbol{q}}_a - 0.01\int(\boldsymbol{q}_a - \boldsymbol{q}_{a,d})dt\ . \quad (4)$$

The gains were empirically tuned to best realize the desired motor positions $\boldsymbol{q}_{a,d} \in \mathbb{R}^2$ on the system.

Several aspects make model-based control of this system challenging. The link inertias are extremely low and hard to determine accurately. Therefore $\boldsymbol{M}$ and $\boldsymbol{C}$ have a high uncertainty. The motor friction $\boldsymbol{\mathcal{Q}}_a$ dominates the motor dynamics and has a high load dependency with a significant stick-slip effect. This is partly compensated by using the motor PID controller of (4) with maximum possible gains. However, many control methods rely on accurate torque control which cannot be implemented on this system. Moreover, the robot's intrinsic stiffness between the base and foot tip changes with its configuration, in contrast to the hopper by Raibert [1]. It is softer when the leg is more contracted and stiffer as the leg straightens [12]. This makes the natural frequency of the robot dependent on configuration and forward velocity. An ideal motor trajectory would excite the robot with this frequency and use its passive dynamics. It is our assumption, that such a trajectory leads to energy-efficient locomotion.

III. Teleoperation Setup and Human Control

A. Control Input

To design an adequate control input for the operator, we chose to control the position of the foot tip $\boldsymbol{x}_f$ w.r.t. $\mathcal{B}$. This resembles controlling the tool center point of a robot in cartesian space. An alternative would be to control the robot's base $\boldsymbol{x}_b$ w.r.t. $\mathcal{F}$. This may be intuitive if the robot is making ground contact, but during the flight phase the base can not be manipulated, so it was rejected. Instead, the chosen control simulates a pushing contact, e.g. pushing one's feet into the ground for liftoff.

As a haptic input device a force dimension® omega.3 with free movement in the xz-plane, cf. Fig. 4a is used. The resulting desired positions of the foot tip $\boldsymbol{x}_d$ are then calculated by:

$$\boldsymbol{x}_d \ = \ \mathrm{SAT}\left(\boldsymbol{K}_S\,\boldsymbol{x}_{o,d} + \begin{bmatrix} 0 \\ 0.22\,\mathrm{m} \end{bmatrix}\right)\ . \quad (5)$$

The function SAT$(\cdot)$ saturates the commanded positions from the omega.3 device $\boldsymbol{x}_{o,d}$ within the workspace of the robot. Further, a diagonal gain matrix $\boldsymbol{K}_S$ is scaling the input and a z-offset compensates for the height of the robot and defines the zero position. The corresponding joint positions $\boldsymbol{q}_{x,d}$ are then derived by inverse kinematics. Note that the desired positions $\boldsymbol{x}_d$ are commanded on the motor side, while the actual foot tip position $\boldsymbol{x}_f$ depends on the link side measurements. With highly elastic systems these two positions differ with a deflected spring, especially during compression. Therefore $\boldsymbol{x}_d$ will not necessarily match $\boldsymbol{x}_f$ during hopping, as the robot will be subject to elastic and link-side dynamics. Consequently, saturated $\boldsymbol{x}_d$ does not imply that $\boldsymbol{x}_f$ is on the edge of the workspace. When the hopper is in compression and about to apply thrust, the saturation of

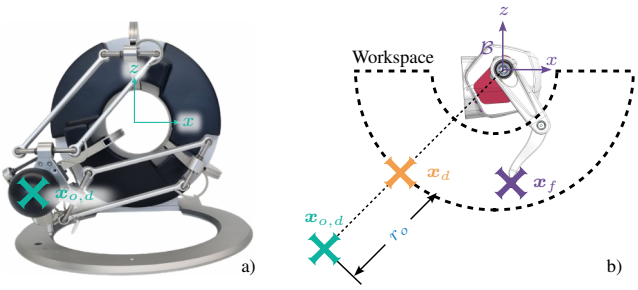

Fig. 4. Fig. 4a shows the omega.3 haptic input device used by the operator to send desired positions $\boldsymbol{x}_{o,d}$. Fig. 4b shows schematically the saturated input $\boldsymbol{x}_d$, distance r_o between $\boldsymbol{x}_{o,d}$ and $\boldsymbol{x}_d$ and actual foot tip position $\boldsymbol{x}_f$.

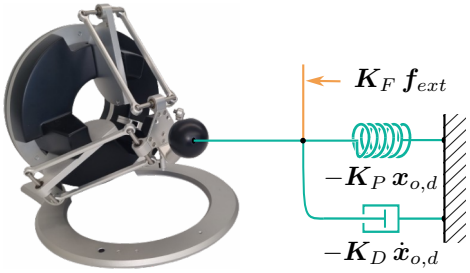

Fig. 5. Schematic of the force feedback signal with virtual spring and damper, and ground reaction force $\boldsymbol{f}_{ext}$.

$\boldsymbol{x}_d$ hinders explosive movements. Energy is transferred from the motors to the links via the spring torques. Limiting the motor positions limits spring torque. Conversely, thrust can be increased by increasing spring deflection. This is done by calculating the distance between the saturated $\boldsymbol{x}_d$ and unsaturated input $\boldsymbol{x}_{o,d}$. This is schematically presented in Fig. 4b. The distance is called r_o and added to $\boldsymbol{q}_{x,d}$. The desired positions for the motor PID controllers in (4) are calculated by:

$$\boldsymbol{q}_{a,d} \ = \ \begin{bmatrix} -k_o\,r_o + 1 & 0 \\ 0 & k_o\,r_o + 1 \end{bmatrix} \boldsymbol{q}_{x,d}\ , \quad (6)$$

where k_o is a positive gain. This feature significantly increased the achievable jumping height and made controlling the robot easier as the operator can choose to inject more energy into the system.

B. Force Feedback

As the operator controls the robot's foot tip, the ground reaction force on the foot tip $\boldsymbol{f}_{ext}$ is chosen as feedback. It conveys the dynamics and behavior of the robot, as it gives information about the compression and thrust of the robot and coincides with the hopping period.

External forces are unknown without extra sensors. Therefore $\boldsymbol{\mathcal{Q}}_{u,j} \cong -\boldsymbol{\tau}_j$ is used as an estimation. This estimation holds with small link inertias and masses and no external forces acting on the base, cf. (1). Projecting $\boldsymbol{\tau}_j$ in $\mathcal{F}$ by the inverse jacobian $\boldsymbol{J}_{\mathcal{F}}$ yields an estimation of the ground

reaction force:

$$\boldsymbol{f}_{ext} \;\cong\; -\left(\boldsymbol{J}_{\mathcal{F}}^{T}\right)^{-1} \boldsymbol{\tau}_j \;. \tag{7}$$

A virtual spring is added to pull the end effector position of the force feedback device $\boldsymbol{x}_{o,d}$ to its zero position. This gives the operator a feel of their position in the workspace of the haptic device. Additionally, a virtual damper ensures stability. Taken together, the force feedback is calculated by:

$$\boldsymbol{f}_{\Omega} \;=\; \boldsymbol{K}_F\, \boldsymbol{f}_{ext} - \boldsymbol{K}_P\, \boldsymbol{x}_{o,d} - \boldsymbol{K}_D\, \dot{\boldsymbol{x}}_{o,d} \;, \tag{8}$$

where the force feedback is scaled by the positive diagonal gain matrices $\boldsymbol{K}_F$, $\boldsymbol{K}_P$ and $\boldsymbol{K}_D \in \mathbb{R}^{2\times 2}$.

C. Controlling the Robot

During operation, the robot is mounted on a boom. This enables translational movement in the robot's xz-plane with fixed rotation of the base. The robot is in sight of the operator and standing in initial configuration, cf. Fig. 2. With increasing input magnitude, the robot starts to jump in place. The jumping height can be controlled by the magnitude of the input while the force feedback guides the operator to the right frequency. With force feedback enabled, the robot can be easily excited with its natural frequency.

Although the foot tip can only be controlled indirectly through the motor positions, the operator still has a high level of control over the robot. By moving the input slightly in the x-direction while jumping, the operator changes the foot tip position relative to the robot's center of mass. This results in a controlled forward motion of the robot. Thus the operator does not need to directly control the foot tip, but rather makes the intuitive connection of position in x-direction and forward speed. With training the operator begins moving the input more in a circle than simply up and down. This results in trajectories that seem to be natural to the system.

IV. Optimizing for Energy-Efficient Locomotion

The operator had the goal of achieving locomotion and generating a desired motor trajectory $\boldsymbol{q}_{a,d}(t)$ for the robot. To save, replay, evaluate and optimize this trajectory, it is fitted to a periodic function and parameterized. To this end, $\boldsymbol{q}_{a,d}(t)$ is cut into n periods and their mean is fitted to a fourth-order Fourier series. The resulting function is called $\text{traj}_0(t, \omega, \varphi) \in \mathbb{R}^2$ and has a modifiable base frequency ω and phase between the two motors φ. This function is plotted and compared with its origin in Fig. 6.

For the optimization, additional scaling A and offset parameters d are introduced:

$$\text{traj}(t, \Theta) = \begin{bmatrix} A_1 \\ A_2 \end{bmatrix} \text{traj}_0(t, \omega, \varphi) + \begin{bmatrix} d_1 \\ d_2 \end{bmatrix} \;, \tag{9}$$

$$\Theta = \{A_1,\, A_2,\, d_1,\, d_2,\, \omega,\, \varphi\} \;. \tag{10}$$

The set Θ contains all six tunable parameters.

The mechanical CoT is used as a measure of energy-efficient locomotion. It is defined by:

$$CoT = \frac{E}{m\, g\, d} \;, \tag{11}$$

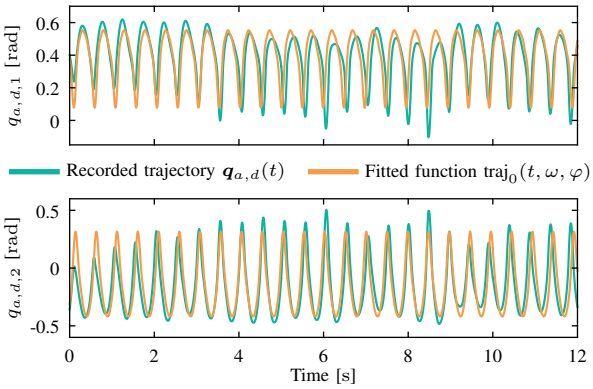

Fig. 6. Recorded motor position trajectory from the operator during hopping and approximation by fourth-order Fourier series.

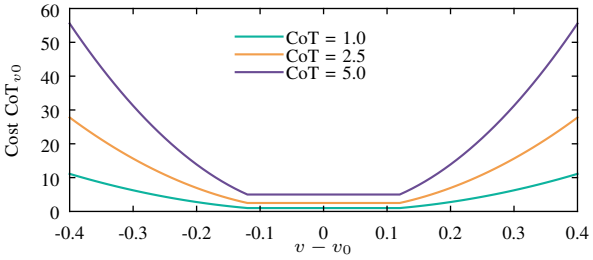

Fig. 7. CoT with weighted velocity CoT_{v0} for different CoT with $k = 0.01$, $v_0 = 0.6$.

with the mass of the robot m, gravitational acceleration g and traveled distance d. For the energy measurement, the combined mechanical output energy of both motors over n periods of length T is used. For SEAs, this is calculated by:

$$E = \int_0^{n\,T} \tau_{j,1}\, \dot{q}_{a,1} + \tau_{j,2}\, \dot{q}_{a,2}\; dt \;. \tag{12}$$

This measurement makes the CoT calculation independent from motor dynamics such as motor friction. Mobile systems tend to have a CoT that is depending on the forward velocity v. Thus optimizing only for CoT without taking v into account makes the results less comparable. Therefore the deviation from the initial forward velocity $v - v_0$ is added as a soft weight in the cost function:

$$\text{CoT}_{v0} \;=\; \text{CoT}\; k^{-1}\, \max\left(k,\; \tilde{v}\right) \;, \tag{13}$$

$$\tilde{v} \;=\; \left(\frac{v - v_0}{2\, v_0}\right)^2 \;, \tag{14}$$

where the max function saturates $\tilde{v}$ on the lower end at $k = 0.01$. Therefore, for small deviations from v_0 and $\tilde{v} \leq k$: $\text{CoT}_{v0} = \text{CoT}$ and the minimum of the cost function is at $\min(\text{CoT})$. For larger deviations, the cost function is rising as depicted in Fig. 7.

V. Results

This section evaluates the performance of the human-generated trajectory in terms of CoT. To this end, it is compared to an optimum of velocity-weighted CoT reached by BBO.

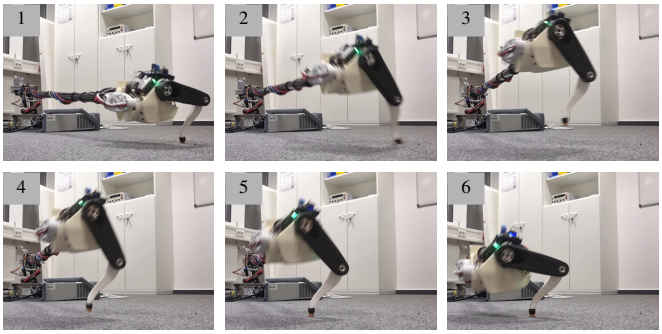

Fig. 8. Snapshots of the hopping monopod with the approximation of the human generated trajectory $\text{traj}_0(t, \omega, \varphi)$.

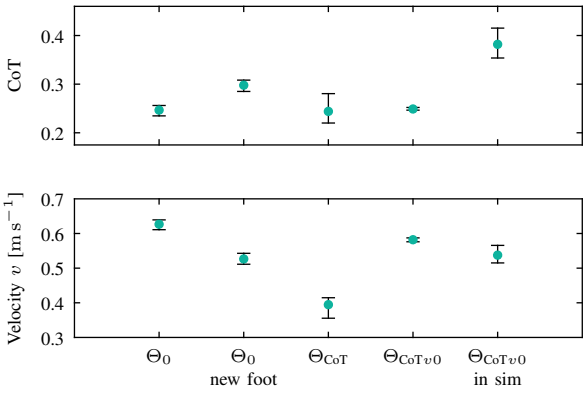

Fig. 9. Resulting CoT and forward velocity when optimizing for CoT and CoT with weighted velocity CoT_{v0} in simulation and on hardware.

A. Evaluation of the Initial Trajectory

Fig. 6 shows a consistent base frequency with the recorded trajectory $\boldsymbol{q}_{a,d}(t)$. It is fitted well by the approximation $\text{traj}_0(t, \omega, \varphi)$ while fluctuations in the amplitude are leveled out. The approximated trajectory is replayed on the robot. It is used as the initial trajectory for the optimization with the parameters Θ_0. A series of snapshots of the resulting hopping gait is presented in Fig. 8.

The CoT is evaluated in trials. Each trial lasts $n = 25$ periods. The first five periods are not evaluated to exclude effects from the previous trial. Fig. 9 shows the mean CoT and forward velocity v over five trials with initial parameters Θ_0 and different optimizations. The error bars are corresponding to the minimal and maximal values. The trajectory with initial parameters has a CoT of 0.25 at $v_0 = 0.63\,\text{m}\,\text{s}^{-1}$. Fig. 1 puts this in comparison with other state-of-the-art robots.

During the experiments, the foot tip of the robot was damaged and changed for a stiffer one. This had a significant impact on the CoT and deteriorated it by $21\,\%$. The generated feed forward trajectory is optimal for the hardware it was created on and sensitive to change. However, changes in stiffness, friction parameters and joint coordinate offsets inevitably occur over time. BBO can be used to maintain optimality.

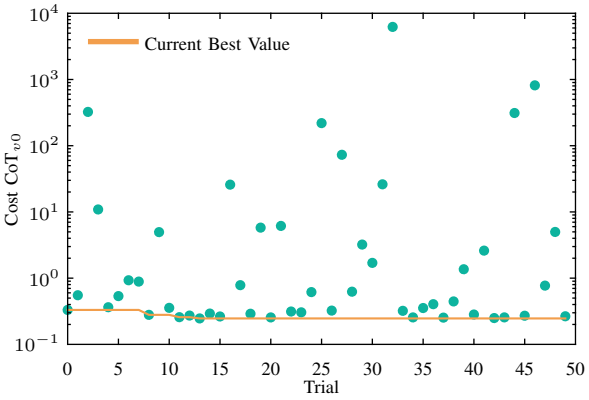

Fig. 10. Optimization history for minimizing CoT_{v0} on hardware.

TABLE II
OPTIMIZED PARAMETERS OF THE DESIRED MOTOR TRAJECTORY

	A_1	A_2	d_1 [rad]	d_2 [rad]	ω [Hz]	φ [s]
Θ_0	1.00	1.00	0.00	0.00	2.04	0.20
Θ_{CoT}	1.11	0.85	0.01	−0.05	1.91	0.21
$\Theta_{CoT_{v0}}$	1.03	1.03	0.02	−0.05	1.96	0.19
Θ_{Sim}	0.86	1.11	0.10	−0.02	2.19	0.18

B. Optimization Setup

The tree-structured parzen estimator algorithm [23] is used, with its implementation from the optuna library [24]. This algorithm was initially developed for hyperparameter optimization. It is sample efficient and therefore suitable for learning on hardware and has shown success on elastic, legged robots [25].

The optimization was performed with the new foot tip. The tunable parameters Θ of the motor trajectory are optimized for minimizing the CoT and for minimizing CoT with weighted velocity CoT_{v0}. The velocity from Θ_0 is used as v_0. An additional third optimization was performed, minimizing CoT_{v0} in simulation with a final evaluation on the hardware. Each optimization was done with 50 trials. Each trial evaluates the cost function for one parameter set. The BBO algorithm finds several good candidates, as depicted in the optimization history in Fig. 10.

C. Evaluation of the Optimization

The results of the optimization in Fig. 9 show, that the margin for improving CoT over the initial trajectory is slim. However, the deterioration of CoT due to hardware changes is compensated. Optimizing for the velocity-weighted cost function CoT_{v0} with the new foot tip brings the CoT and forward velocity v in close vicinity to the initial values with the old foot tip. Whereas optimizing only for CoT results in a slower v, underlining the need for the combined cost function. Sim to real transfer was not successful for this system as indicated by a high CoT with $\Theta_{\text{CoT}v0}$ in simulation. This shows the need for either an accurate model or optimizing directly on the hardware. The latter is useful if an accurate model can not be obtained as was done in this work.

The best parameter set of each optimization is presented in Table II with the cost function denoted in their respective indices. The parameters for the different optimizations are in proximity to the initial values. They have a frequency around $\omega \approx 2\,\mathrm{Hz}$ and differ slightly in scaling A and offset d. We conclude that the initial parameters are already energy efficient and ω matches the natural frequency of the system for hopping for $v \approx v_0$. Further, the CoT and v are sensitive to these parameters.

VI. Conclusion

For the first time, a method of controlling an elastic hopper by teleoperation was presented to generate motor trajectories. By using an approximation of the ground reaction force as force feedback, the operator is guided to match the trajectory to the natural frequency of the hopper. These generated motor trajectories, when replayed on the robot, produce a hopping gait that is close to optimal in terms of cost of transport. Optimality was confirmed by black-box optimization. Slight hardware changes affect the optimality of the initial trajectory, which is compensated by the optimization.

We plan to use the presented method on other highly elastic mobile robots such as hoppers with built-in structural elasticity and elastic snakes. Future works may also investigate reinforcement learning methods to transfer the results on the broader class of monopods that have an unlocked hip rotation.

References

[1] M. H. Raibert, *Legged robots that balance*, ser. The MIT Press series in artificial intelligence. Cambridge, Mass: MIT Press, 1986.

[2] J. Grimes and J. Hurst, "The Design of Atrias 1.0 a Unique Monopod, Hopping Robot," in *Adaptive Mobile Robotics*. WORLD SCIENTIFIC, Sep. 2012, pp. 548–554.

[3] P. Gregorio, M. Ahmadi, and M. Buehler, "Design, control, and energetics of an electrically actuated legged robot," *IEEE Trans. Syst., Man, Cybern. B*, vol. 27, no. 4, pp. 626–634, Aug. 1997.

[4] M. Ahmadi and M. Buehler, "The ARL monopod II running robot: control and energetics," in *Proceedings 1999 IEEE International Conference on Robotics and Automation (Cat. No.99CH36288C)*, vol. 3. Detroit, MI, USA: IEEE, 1999, pp. 1689–1694.

[5] X. Liu, A. Rossi, and I. Poulakakis, "A Switchable Parallel Elastic Actuator and its Application to Leg Design for Running Robots," *IEEE/ASME Trans. Mechatron.*, vol. 23, no. 6, pp. 2681–2692, Dec. 2018.

[6] S. Seok, A. Wang, Meng Yee Chuah, D. Otten, J. Lang, and S. Kim, "Design principles for highly efficient quadrupeds and implementation on the MIT Cheetah robot," in *2013 IEEE International Conference on Robotics and Automation*. Karlsruhe, Germany: IEEE, May 2013, pp. 3307–3312.

[7] A. Schmidt, F. Pasic, D. Calzolari, A. Sachtler, T. Gumpert, M. Keppler, and A. Albu-Schäffer, "Comparison of control strategies to excite intrinsic oscillations in a sea-driven robotic joint," in *2024 European Control Conference (ECC)*, 2024, pp. 2194–2199.

[8] Y. Kurita, Y. Matsumura, S. Kanda, and H. Kinugasa, "Gait patterns of quadrupeds and natural vibration modes," *Journal of System Design and Dynamics*, vol. 2, no. 6, pp. 1316–1326, 2008.

[9] R. M. Ghigliazza, R. Altendorfer, P. Holmes, and D. Koditschek, "A Simply Stabilized Running Model," *SIAM J. Appl. Dyn. Syst.*, vol. 2, no. 2, pp. 187–218, Jan. 2003, publisher: Society for Industrial and Applied Mathematics.

[10] H. Geyer, A. Seyfarth, and R. Blickhan, "Spring-mass running: simple approximate solution and application to gait stability," *Journal of Theoretical Biology*, vol. 232, no. 3, pp. 315–328, Feb. 2005.

[11] B. Andrews, B. Miller, J. Schmitt, and J. E. Clark, "Running over unknown rough terrain with a one-legged planar robot," *Bioinspir. Biomim.*, vol. 6, no. 2, p. 026009, Jun. 2011.

[12] R. Blickhan, "The spring-mass model for running and hopping," *J Biomech*, vol. 22, no. 11-12, pp. 1217–1227, 1989.

[13] D. Calzolari, C. D. Santina, A. M. Giordano, and A. Albu-Schäffer, "Single-Leg Forward Hopping via Nonlinear Modes," in *2022 American Control Conference (ACC)*, Jun. 2022, pp. 506–513, iSSN: 2378-5861.

[14] S. Faraji, S. Pouya, R. Moeckel, and A. J. Ijspeert, "Compliant and adaptive control of a planar monopod hopper in rough terrain," in *2013 IEEE International Conference on Robotics and Automation*, May 2013, pp. 4818–4825, iSSN: 1050-4729.

[15] D. Ahn and B.-K. Cho, "Optimal Periodic Hopping Trajectory Generation for Legged Robots," in *2018 IEEE/ASME International Conference on Advanced Intelligent Mechatronics (AIM)*. Auckland: IEEE, Jul. 2018, pp. 1263–1268.

[16] M. Hutter, C. D. Remy, M. A. Hopflinger, and R. Siegwart, "SLIP running with an articulated robotic leg," in *2010 IEEE/RSJ International Conference on Intelligent Robots and Systems*. Taipei: IEEE, Oct. 2010, pp. 4934–4939.

[17] C. Lee and S. Oh, "Development, Analysis, and Control of Series Elastic Actuator-Driven Robot Leg," *Front. Neurorobot.*, vol. 13, p. 17, May 2019.

[18] R. Ringrose, "Self-stabilizing running," in *Proceedings of International Conference on Robotics and Automation*, vol. 1, Apr. 1997, pp. 487–493 vol.1.

[19] C. Hubicki, J. Grimes, M. Jones, D. Renjewski, A. Spröwitz, A. Abate, and J. Hurst, "ATRIAS: Design and validation of a tether-free 3D-capable spring-mass bipedal robot," *The International Journal of Robotics Research*, vol. 35, no. 12, pp. 1497–1521, Oct. 2016.

[20] S. Schaal, C. G. Atkeson, and D. Sternad, "One-Handed Juggling: A Dynamical Approach to a Rhythmic Movement Task," *Journal of Motor Behavior*, vol. 28, no. 2, pp. 165–183, Jun. 1996, publisher: Routledge _eprint: https://doi.org/10.1080/00222895.1996.9941743.

[21] A. Schmidt, M. Forano, A. Sachtler, D. Calzolari, D. Franklin, and A. Albu-Schäffer, "Finding the rhythm: Humans exploit nonlinear intrinsic dynamics of compliant systems in periodic interaction tasks," Neuroscience, preprint, Sep. 2023.

[22] D. Lakatos, K. Ploeger, F. Loeffl, D. Seidel, F. Schmidt, T. Gumpert, F. John, T. Bertram, and A. Albu-Schäffer, "Dynamic Locomotion Gaits of a Compliantly Actuated Quadruped With SLIP-Like Articulated Legs Embodied in the Mechanical Design," *IEEE Robotics and Automation Letters*, vol. 3, no. 4, pp. 3908–3915, Oct. 2018, conference Name: IEEE Robotics and Automation Letters.

[23] J. Bergstra, R. Bardenet, Y. Bengio, and B. Kégl, "Algorithms for Hyper-Parameter Optimization," in *Advances in Neural Information Processing Systems*, vol. 24. Curran Associates, Inc., 2011.

[24] T. Akiba, S. Sano, T. Yanase, T. Ohta, and M. Koyama, "Optuna: A Next-generation Hyperparameter Optimization Framework," Jul. 2019, arXiv:1907.10902 [cs, stat].

[25] A. Raffin, D. Seidel, J. Kober, A. Albu-Schäffer, J. Silvério, and F. Stulp, "Learning to Exploit Elastic Actuators for Quadruped Locomotion," Aug. 2023, arXiv:2209.07171 [cs].